COMPARISON OF DIAGNOSTIC METHODS FOR NONEQUILIBRIUM PLASMA-JET WIND TUNNEL FLOW*

By Chul Park**

ABSTRACT

Various experimental methods for determining the state of gas flow in chemical nonequilibrium throughout a plasma-jet wind tunnel are compared. These methods are (i) using energy balance to determine gross enthalpy, (ii) using stagnation chamber pressure and mass flow rate relation to determine plenum chamber enthalpy, (iii) measuring convective heat transfer with a blunt and a slender model to determine test-section enthalpy, (iv) using shock-wave standoff distance to determine ionization or dissociation fractions, (v) using radiative heat transfer probe to determine electron density, and (vi) using spectroscopy to determine electron temperature.

The experimental data were obtained in a 1-inch plasma-jet wind tunnel, using argon and nitrogen as working gases, with a stagnation chamber pressure of approximately 1/3 atmosphere. Reynolds number and Mach number at the exit of the tunnel were approximately 1000 and 3,

---

*This is extracted from the Ph.D. thesis of the author submitted at the Imperial College of Science and Technology, London, England.

**Research Associate of the National Academy of Sciences - National Research Council with the NASA, Ames Research Center, Moffett Field, California.

respectively. The various experimental data were compared by means of theoretical flow calculations (i) for ionized argon by solving the nozzle flow ionic relaxation problem with a computer, and (ii) for dissociated nitrogen using the frozen flow relations. The conclusions drawn include: (i) for argon, the various methods of diagnosis are consistent, (ii) in nitrogen, the sum of kinetic energy of the gas and the dissociational energy is significantly less in a weakly dissociated regime than the total energy which is recovered by the heat transfer to a test body, and (iii) the three-body recombination rate of Hinnov and Hirschberg and the two-body recombination rate of Bond in ionized argon are accurate within the experimental accuracy in a flow expanding through a nozzle.

INTRODUCTION

As a means of simulating reentry into planetary atmospheres, plasma-jet, or arc-heated, wind tunnels have been developed in recent years in great variety.[1] The experimental data obtained to date in plasma-jet wind tunnel facilities show, however, contradictions, conflicts, and a general lack of conformity. In particular, the energy levels obtained by various diagnostic methods do not agree under certain circumstances.[2] Although certain types of experiments, such as heat transfer measurements, show reasonable agreement with what is expected, some types of experiment such as chemical reaction rates[3,4] show results that apparently are in error by several orders of magnitude. These inconsistencies have so far been attributed mainly to experimental errors rather than to systematic discrepancies. Because,

however, some of the discrepancies amount nearly to 80 percent of a total value,[2] experimental results obtained with a plasma-jet wind tunnel may be subject to considerable uncertainty unless the nature of such discrepancies is identified and explained.

The purpose of the present paper is to identify such systematic discrepancies as may be present among usual diagnostic techniques, and to assess their extent. One may note that the reported inconsistencies appear more frequently in facilities using nitrogen gas than those using argon gas, and also that uncertainties arise partly because a limited number of diagnostic methods were used in a given investigation. In an attempt to clarify the difference between the two gases, therefore, in the present work, tests with both nitrogen and argon were performed with the same techniques. Also, to provide a redundancy of data that would permit detection of which technique yields anomalous results, six different diagnostic methods were tried. These were (i) energy balance to determine gross enthalpy, (ii) settling chamber pressure and mass-flow rate relation to determine plenum chamber enthalpy, (iii) convective heat transfer measurement with a blunt and a slender model to determine test-section enthalpy, (iv) shock-wave standoff distances to determine ionization and dissociation fractions, (v) radiative heat-transfer measurements to determine electron density, and (vi) spectroscopy to determine electron temperature. Experimental data from the various diagnostic methods were compared by means of theoretical calculations. To minimize the portion of the study dealing with the heat transfer we omit the detailed calculation procedures and simply

refer to the work previously published.[5,6] The paper concludes that systematic discrepancies exist among the various methods for determining enthalpy with nitrogen but not with argon when all the factors are properly accounted for. It also appraises the types of experiments that are apparently free of such discrepancies.

EXPERIMENTAL APPARATUS AND PROCEDURE

Wind Tunnel

The wind tunnel is a Plasmadyne AM-3 supersonic plasma jet assembly having throat and exit diameters of 0.447 and 0.836 inch, respectively. The expanding portion of the nozzle is aerodynamically contoured and has an approximately conical semivertex angle of 6° that is followed by a parallel portion of a length of one exit diameter, as shown in Fig. 1. Argon and nitrogen were test gases, and the operating range of the tunnel was as follows:

With argon:

$0.14 < \dot{m} < 0.3$ lb/min

$10 < E < 50$ kw

$0.18 < p_o < 0.45$ atm

$5\times10^{-4} < \rho_\infty < 1.5\times10^{-3}$ amagat

With nitrogen:

$0.07 < \dot{m} < 0.2$ lb/min

$15 < E < 80$ kw

$0.15 < p_o < 0.4$ atm

$3\times10^{-4} < \rho_\infty < 2\times10^{-3}$ amagat

The effective nozzle exit area ratio determined from the impact pressure was approximately 2.7. Other operating characteristics of the tunnel are described in references 7 and 8.

Records of instantaneous voltage and current show that the arc is stable when operated with argon but fluctuates mildly when operated with nitrogen.[8] The wearing rate of the water-cooled electrodes was not measurable for argon but was of the order of 1/2 lb per 100 lb of gas for nitrogen. Accumulation of electrical charge on the model surface due to rarefied-plasma effect was not present for any of the models used during the operation of the tunnel.

Power Balance

Power balance provides a measure of the gross energy content of the gas. One measures the electrical power input to the arc electrodes, E, and the heat rejected to the water cooling the electrodes and settling chamber, W. The gross enthalpy, denoted by H_{tpb}, is then determined from

$$H_{tpb} = \frac{E - W}{\dot{m}} \equiv \overline{\eta} \frac{E}{\dot{m}}$$

where $\dot{m}$ is the total mass flow. One then refers to a Mollier diagram to determine other presumably equilibrium properties in the settling chamber. This method of determining enthalpy is based on the first law of thermo-dynamics, and provides an <u>average</u> enthalpy value composed only of measured quantities.

Pressure and Mass-Flow Relation

The method enabling the determination of enthalpy level from the measurement of settling chamber pressure and mass-flow rate through the aerodynamically choked nozzle is termed here pressure--mass-flow method. The enthalpy so obtained, denoted H_{tmf}, is also a bulk value that is a measure of the thermal energy available in, and for conversion to, kinetic form.

The one-dimensional equations of continuity and energy through the nozzle can be rearranged for argon to yield the frozen stagnation enthalpy as

$$h_o = 2.5 \left(\frac{\Gamma p_o A_*}{\dot{m}} \right)^2$$

where Γ is the nozzle coefficient defined as

$$\Gamma = \frac{\rho_*}{\rho_o} \frac{u_*}{\sqrt{(1 + \varphi_o) R T_o}}$$

The nozzle coefficient, Γ, for argon was calculated from the results of nozzle flow properties computed by Bray's method[9] with the three-body recombination rate of Hinnov and Hirschberg.[10,11] The relaxation of electron temperature was computed from the relaxation rate[12] under the assumption that the departure of electron temperature from atom temperature was small. The results of these computations are shown in Figs. 2(a) to 2(c). The nozzle coefficient, Γ, was found to be approximately 0.725.

To determine the effective sonic throat area, A*, the displacement thickness of the boundary layer at the throat was calculated by the method of Cohen and Reshotko.[13] The calculation shows that the

displacement thickness at the throat is negative and amounts to approximately 3 percent of the geometric throat radius for a typical operating condition.

The frozen enthalpy was determined for argon, using the above relations, and the corresponding total enthalpy H_{tmf} was found from a specially drawn Mollier diagram which includes the values of frozen enthalpy.[5] The negative displacement area increased the total enthalpy levels calculated by the pressure--mass-flow method by as much as 50 percent at high enthalpy levels as compared to a corresponding enthalpy calculated by means of the geometric throat area.

For nitrogen, calculations using the freezing criteria of references 14 and 15 show that the vibrational de-excitation is frozen in the convergent, subsonic portion of the nozzle. Also, with the freezing criterion of Bray,[16] dissociation is found to be frozen at low subsonic Mach numbers. For the sake of simplicity, therefore, both vibration and dissociation were assumed to be frozen at the settling chamber values, and conservation relations for completely frozen flows were utilized to calculate nitrogen gas enthalpy by the pressure--mass-flow method. The specific heat determined by

$$C_p = (3.5 + 1.5\alpha)R$$

was used to compute the settling chamber enthalpy from the ideal dissociating gas relations of Lighthill[17] as a function of the settling chamber pressure and mass-flow rate. The results are presented in reference 5. In the pressure--mass-flow method for nitrogen, therefore,

the enthalpy H_{tmf} was read directly from the approximate chart in reference 5, using measured values of $\dot{m}$, and p_o as inputs.

The enthalpy levels calculated by the power balance method and pressure--mass-flow method are shown in Figs. 3 and 4. In Fig. 3, two methods are compared by their resulting tunnel head efficiency $\overline{\eta}$ (see the equation in the preceding paragraph). Here the large scatter in the H_{tpb} data is due to the instrument inaccuracy for wind tunnel operation with argon. As seen from Fig. 3, the two methods agree for argon within the possible experimental accuracy. For nitrogen, Fig. 4 shows a significant difference at lower enthalpy levels; that is, the enthalpy values determined by the pressure--mass-flow method, which represents the sum of kinetic energy and the dissociation energy of the gas, is less than the value obtained by power balancing which denotes the gross energy content.

In the description of the results, the measurements in argon are plotted against $E/\dot{m}$ because this procedure minimizes the scattering of test data due to instrument error mentioned above. Enthalpy can be recovered from each $E/\dot{m}$ value by multiplying by the corresponding efficiency given in Fig. 3. For the operation with nitrogen, this procedure was unnecessary and so the original data were obtained with reference to H_{tpb}.

Convective Heat-Transfer Measurement

The heat-transfer probes were a hemisphere and a 15° semiangle cone both of 0.4-inch diameter, and were water cooled inside.[5] The steady-state total heat transfer rate to either the hemispherical or

conical portion of the body was determined by measuring the temperature rise of the cooling water. Copper, chromium, stainless steel, and two different ceramic coatings were used as model surfaces. The ceramic coatings were industrial, high-temperature boro-silicate Ferro 571 on the copper surface, and Ferro 5210-C on the stainless steel surface.[18] They were manufactured by Ferro Enamels, Ltd., England, and were from 0.001 to 0.003 inch thick.

Increases in catalytic activity among the various surfaces may result in corresponding increases of heat-transfer rate response that can be related to the recombination of dissociated species. This information can be interpreted by means of theory to determine whether or not the flow past the probes is in a state of chemical equilibrium.[19] The gross heat-transfer rate measurements, of course, yield data that, along with impact-pressure measurements, can be related to total enthalpy by appeal to various laminar heat-transfer theories.[19,20] This technique yields a value of total enthalpy characteristic of the stream tube within which the measurements are made, and the value so determined, H_{thx}, is compared with H_{tpb} on Fig. 4.

The results of convective heat-transfer rate measurements are shown in Figs. 5 and 6 and are compared with the theoretical values. In Figs. 5 and 6, the measured heat-transfer rate Q is divided by $\sqrt{\dot{m}}$, because $\dot{m}$ is proportional to the relevant Reynolds number and yet is more directly obtainable than the Reynolds number. In the measurement of the convective heat-transfer rates, the additional heating by radiation was neglected because it is small. The theoretical values for argon are based on the solutions of nozzle flow calculations shown in

Figs. 2(a) to 2(c) and the solutions of the boundary-layer heat-transfer equations for equilibrium and frozen flows.[6] The theoretical values for nitrogen are derived from the following considerations:

(i) Yos's data[21] are used for the transport properties,

(ii) Fay and Riddell's data[20] are used as the basic solution of boundary-layer heat-transfer equations,

(iii) Vorticity interaction effect is corrected by Van Dyke's data,[22]

(iv) Goulard's frozen flow theory[19] was used to calculate the surface recombination effect. This was done because a detailed calculation of the atom concentration within the shock layer using the method of reference 23 shows an almost frozen flow throughout. For both argon and nitrogen, the local heat transfer rate distribution over the hemisphere is taken from the work of Kemp, Rose, and Detra.[24]

The experimental results for argon with the conical body agree approximately with theoretical heat transfer rates shown in Fig. 5(a) under the labeling $k = 5\times10^{27}T^{-4.5}cm^{6}mole^{-2}sec^{-1}$. This means that if the enthalpy level is calculated from the measured heat-transfer rate, the results will agree with H_{tpb} or H_{tmf}. The heat-transfer rate to a hemisphere in an ionized argon flow is sensitive to the electron density when the boundary layer is ionically frozen.[6] Hence, the fact that the measured values agree approximately with the theoretical values based on H_{tbp} or H_{tmf} indicates that not only the total enthalpy but the electron density thus determined must agree with those values predicted by H_{tpb} or H_{tmf}.

The energy levels in nitrogen deduced from the measured heat-transfer rates for copper models assuming $k_w = 0.063T_w$ (see ref. 11)

were illustrated previously in Fig. 4. As seen from Fig. 4, the test results agree roughly with the values based on the power balance method.

Shock-Wave Standoff Distance

Illumination pictures of the shock layer over the hemispheric probe are shown in Fig. 7(a). The densitometer trace shown in Fig. 7(b) is obtained by scanning the negative of the picture across the stagnation region of the shock layer. The abscissa in the densitograph is the distance along the stagnation streamline; the ordinate represents the brightness of the gas at a point on the stagnation streamline, and is related to the density of the negative by a nonlinear function. The shock-wave position is determined either by extrapolating the trace of the densitograph as in Fig. 7(b) or by measuring the distance directly from the negative using a traversing microscope.

The results of measuring the standoff distance are shown in Figs. 8 and 9. The experimental results are higher than the theoretical values based on inviscid flow assumptions, even at lowest enthalpy levels where the theory should agree with the experiment under all circumstances. This is thought to be due to the large model-to-jet diameter ratio. In interpreting the experimental data, therefore, we account for this effect by adding the same arbitrary distance to each of the theoretical values (as shown on the figures) so that each agrees with experimental results at low enthalpy levels. By a simple logical deduction,[11] one can prove that for such flow conditions as prevailed in the present study, the standoff distance of a shock wave in argon is determined mainly by ionic recombination in the nozzle, whereas in a

nitrogen flow, the standoff distance indicates the frozen dissociation level. Figure 8 shows that the measured standoff distances in argon agree best with theoretical calculations based on the parameters of relaxing flow shown in Figs. 2(a) to 2(c). In the calculation of the shock standoff distances shown, the flow behind the bow shock wave was assumed to be in equilibrium at the enthalpy determined from the power balance measurements. A more elaborate estimation of shock standoff distance[23] has shown that this flow, indeed, closely approaches equilibrium. Figure 10 shows that the measured standoff distances in nitrogen agree with the theoretical values of frozen flow. The agreement proves that the dissociation levels calculated by the power balance method are consistent.

Radiative Heat Transfer

The radiative heat transfer from the exit jet flow of the wind tunnel was measured with a windowless, differential bolometer (Fig. 10). The sensing elements were two brass foils of 3/16-inch diameter and 0.002 inch thick placed 1/2-inch apart. The sensing face of the main element, that is, the element directly exposed to the radiation, was blackened by lamp-black. Six large holes were drilled through the bolometer housing, which was made of PTFE (Polytetrafluorethylene), to permit ready access of the surrounding gases to all faces of the elements. Radiative heat-transfer rate is determined from the temperature difference between the two elements. With this design, the convective heat transfer to both elements annul each other and only the difference in radiative heat transfer is detected.

The bolometer was calibrated by exposing it to an electrically heated radiator under the same vacuum condition as existed during the test, that is, a static pressure of 5 mm Hg. The electrical heater was placed exactly in the position of the measured gas stream.

It is known that for a moderately ionized regime, that is, when the electron concentration is of the order of 10 percent, the two-body, free-bound transition of electrons is the dominating mechanism of radiation.[25] The intensity of radiation by the free-bound transition is proportional to the square of absolute electron density, the constant of proportionality being a function of temperature. Thus, by using a theoretical formula, such as Bond's,[25] to relate the intensity with the absolute electron density, one can calculate the electron concentration and hence the state of the gas, provided the nozzle flow relations are known for each equilibrium settling chamber condition.

The results of the radiative heat-transfer rate measurements are shown in Figs. 11(a) and 11(b). For the results with argon, the experimental values are compared with the theoretical values for the two-body, free-bound transition theory of Bond,[25] calculated using the nozzle flow properties presented in Figs. 2(a) to 2(c). Figure 11(a) shows that for argon the experimental results agree with the theoretical values within approximately 30 percent at moderate ionization levels where Bond's theory is applicable. For low ionization levels, the bound-bound transitions dominate and so Bond's theory is not applicable. The enthalpy levels calculated from this measurement are therefore higher than those calculated by power balance, pressure--mass-flow, or heat-transfer-probe methods. This discrepancy is thought to be due mainly

to the error in the theory. Since the theory of Bond is subject to the error of this order, one cannot expect at this stage any better agreement than the present result. Since the radiation intensity is proportional to the square of electron density, however, the flow state calculated by the radiation measurement yields values only approximately 15 percent higher than those calculated by other methods.

For nitrogen, the theoretical values obtained by extrapolating Yos's data,[21] with the assumptions that the flow through the nozzle is completely frozen and that the radiation comes entirely from the free-bound transitions, are smaller than the experimental results by several orders of magnitude (Fig. 11(b)). Since the other source of radiation at these temperature ranges, that is, the bound-bound transitions, also fails to explain such a large amount of radiation, it leaves only one other possible mechanism for the observed radiation, that is, the presence of metastable states (see Discussion).

Spectroscopy

The spectroscopic measurements were carried out by Adcock and Plumtree[26] for argon flow and the results of their work are used here for comparison. They measured the relative intensities of neutral atom lines for argon in the empty test section for the wave-length range from 3800 to 5400Å, corresponding to the transitions from quantum states close to ionization. The temperatures obtained from their measurements are believed, therefore, to be those of electrons (see, e.g., ref. 27).

The results of spectroscopic temperature measurement carried out by Adcock and Plumtree[26] for argon are compared in Fig. 12 with

corresponding results based on the power balance, pressure--mass-flow method and the nozzle flow calculation shown in Figs. 2(a) to 2(c). As seen from Fig. 12, the measured electron temperatures agree roughly with the values calculated using the ionic recombination rate of Hinnov and Hirschberg, $k = k$.

For nitrogen, Adcock and Plumtree did not resolve quantitative values of temperature. However, they found that there was no appreciable population of nitrogen ions, which means that any radiation present in the stream was not due to free-bound transitions of electrons (see Discussion).

DISCUSSION

The results of the experiments described in the preceding sections are summarized in table 1. As indicated in the table, each type of experiment measures a different quantity and comparison is possible only when appropriate theories are used, the proper theory being decided by the criterion used in the comparison. It was not possible to find a common state parameter for comparing all types of measurement that would exhibit the differences among them to an equal degree of accuracy. For instance, even though the shock-wave standoff distance is a direct indication of atom concentration and hence the energy level of dissociated nitrogen at high enthalpy levels, it is insensitive to changes in enthalpy at low energy levels where the power balance method and pressure--mass-flow method apparently deviate from each other. Therefore in the comparison of the results, different criteria are used for each type of experiment, and the figure illustrating each comparison

best is indicated in the table. As seen from the table, the results in argon are well consistent, but the results in nitrogen are not (i.e., they deviate from the idealistic condition).

One of the inconsistencies in the nitrogen results is that the shock-wave standoff distance agrees with the power balance method. Since the unknown latent energy would not change the atom concentration, the standoff distance should always agree with the theory based on the pressure--mass-flow method. This inconsistency is thought to be due, however, to the incapability of resolving the flow enthalpy levels by the standoff distance measurement at low enthalpy levels. Since for a high-enthalpy range the power balance method yields the same enthalpy values as the pressure--mass-flow method, the results should indeed be interpreted as showing the agreement between the enthalpy levels determined by shock-wave standoff distance and pressure--mass-flow method.

For argon, the experimental results obtained with the six different diagnostic methods described agree with each other. Therefore, the agreement proves that the following underlying theories are right to the accuracy achieved in the experiments:

(i) The assumption of thermal and ionic equilibrium in the settling chamber,

(ii) The calculation of ionic and electron temperature relaxation process as in nozzle,

(iii) The three-body ionic recombination rate of Hinnov and Hirschberg,[10]

(iv) The two-body ionic recombination rate of Bond,[25]

(v) The postulation that the relative line intensities among the lines of high principal quantum number states tend to be in equilibrium with the electron temperature, and

(vi) The solutions of boundary layer heat-transfer equations for ionized argon by Park.[6]

For nitrogen flow, the following two inconsistencies exist: that is,

(i) The pressure--mass-flow method underestimates the energy level considerably at low enthalpy levels,

(ii) The radiation from the gas is several orders of magnitude more intense than theory predicts.

The first point supports the findings of Arney and Boylan. They report[4] that an extraordinarily large-sized settling chamber, a size which is far greater than any reasonable de-excitation length, is necessary to make the power balance and pressure--mass-flow methods agree at low enthalpy levels.

One possible cause of the energy discrepancy in nitrogen might be the effect of metallic ions present in the gas stream. The copper contaminants in the gas, which have already absorbed 3.29 ev for gasification, may completely ionize, and remain so until they pass the throat, resulting in the absorption of 11.3 ev per molecule in total. The portion of energy absorbed by this phenomenon is not included in H_{tmf} and so it may differ from H_{tpb} by this amount. Figure 5 therefore shows the effect of 2.5 percent copper contamination by volume when the complete ionization of copper atoms is assumed. As seen from Fig. 5, it is necessary to have approximately 2.5-percent contamination to account

for the large energy difference at low enthalpy levels. Since the actual wearing rate of the electrodes was approximately 1/10 of this amount, it is not likely that the contaminant ionization is the main cause of the observed discrepancy.

A more likely cause of the two inconsistencies observed is that there is a significant population of gas atoms and molecules in metastable states. Since nitrogen has particularly abundant metastable states and because some of them occur at quite low energy levels, it is possible that a significant portion of the electrical energy initially put into the gas is locked in the form of metastable states. Because a great length of time is required for an electron in a metastable state to transfer to the ground states, a large settling chamber would be necessary to establish complete equilibrium. Thus the findings of Arney and Boylan[4] appear reasonable. The retarded transition from the metastable states also may result in augmented radiation from the expanded flow and this possibly explains the large measured value of radiation. Recently, some unpublished evidence supporting the existence of the metastable states was found by Drellishak and Winkler. They observed the line and band emissions from nitrogen behind a normal shock wave in a frozen flow and found the rate of production of ionized nitrogen molecules behind the shock wave to be several orders of magnitude greater than that observed in a shock tube. This phenomenon can be explained by the presence of metastable gases in large quantity.

CONCLUSIONS

1. For argon, the method of Bray (ionized plasma-jet wind tunnel flow based on the assumption of equilibrium settling chamber condition) is useful as the basis for determining the flow condition in a plasma-jet wind tunnel.

2. For argon, the power balance, pressure--mass-flow method, and the heat-transfer measurements to a blunt and a slender body are all consistent; hence any of the three methods can be used to determine the flow conditions as long as the displacement thickness at the throat is properly accounted for.

3. For argon, the three-body recombination rate of Hinnov and Hirschberg and the two-body recombination rate of Bond are accurate within the experimental accuracy for the flow expanding in the plasma-jet wind tunnel nozzle.

4. For nitrogen, there is an unknown mechanism of energy absorption by the gas, likely in the form of metastable species. These species comprise a significant portion of the total energy at low enthalpy levels. This energy is recoverable as heat transfer to a catalytic surface, and so the power balance method and the heat-transfer measurement agree but the pressure--mass-flow method does not.

5. The standoff distance of a shock wave over a hemisphere can be used to determine the atom concentration in the stream in a near frozen flow.

ACKNOWLEDGMENT

The author wishes to express his sincere thanks to Mr. J. L. Stollery of Imperial College of Sciences and Technology, London, England, for his inspiring supervision and kind interest.

NOMENCLATURE

A	cross-sectional area of wind-tunnel nozzle
E	electrical power input to arc
H	enthalpy, that is, sum of frozen enthalpy h and energy of dissociation or ionization
H_t	total enthalpy, that is, enthalpy plus kinetic energy and other forms of energy, if any
H_{thx}	H_t determined by heat transfer measurement
H_{tmf}	H_t determined by pressure--mass-flow method
H_{tpb}	H_t determined by power balance method
h	frozen enthalpy C_pT
k	ionic recombination rate constant
k_w	surface catalytic recombination rate constant
$\dot{m}$	mass-flow rate through wind-tunnel nozzle
p	pressure
Q	convective heat-transfer rate
R	radius of hemisphere for Figs. 8 and 9; elsewhere, gas constant
T	heavy particle temperature
T_ϵ	electron temperature
u	velocity

W power rejected to cooling water

α atom concentration

Δ standoff distance of shock wave

$\overline{\eta}$ efficiency of plasma-jet arc heater

ρ density

φ ionization fraction

Subscripts

E equilibrium value

F frozen value

o settling chamber

w wall surface of test body

∞ condition in the test section

$*$ condition at throat of nozzle

REFERENCES

1. Cordero, J., F. W. Dietrich, and H. Hurwicz, Description of Aerothermodynamic Test Facilities and Techniques for the Evaluation of Reentry Structures and Materials, Aerospace Engineering, 1963, 22, 266-289.

2. Winkler, E. L., and R. N. Griffin, Jr., "Effects of Surface Recombination on Heat Transfer to Bodies in a High Enthalpy Stream of Partially Dissociated Nitrogen," NASA TN D-1146, 1961.

3. Chen, C. J., Experimental Investigation of Atomic Recombination in a Supersonic Nozzle, Jour. of Fluid Mechanics, 1963, 17(3), 450-458.

4. Arney, G. D., Jr., and D. E. Boylan, "A Calorimetric Investigation of Some Problems Associated With a Low-Density Hypervelocity Wind Tunnel," AEDC-TDR-63-19, 1963. Also see Lewis, A. D., and G. D. Arney, "Vibrational Nonequilibrium With Nitrogen in Low-Density Flow," AEDC-TDR-63-31, 1963.

5. Park, C., "Measurement of Heat Transfer to a Hemisphere in High Enthalpy Argon and Nitrogen Streams in a Plasma Jet Wind Tunnel," British ARC 24, 948, April 1963.

6. Park, C., Heat Transfer From Nonequilibrium Ionized Argon Gas, AIAA Jour., 1964, 2(1), 169-171.

7. Harvey, J. K., and P. G. Simpkins, A Description of the Imperial College Arc-Heated Wind Tunnel, Jour. of Royal Aeronautical Sci., 1962, Oct., 66, 637-641.

8. Harvey, J. K., P. G. Simpkins, and B. D. Adcock, Instability of Arc Columns, AIAA Jour., 1963, 1(3), 714-715.

9. Bray, K. N. C., Electron-Ion Recombination in Argon Flowing Through a Supersonic Nozzle, in the High Temperature Aspects of Hypersonic Flow, AGARDograph 68, W. C. Nelson Ed., New York, Pergamon, 1964, 67-84.

10. Hinnov, E., and J. G. Hirschberg, Electron-Ion Recombination in Dense Plasmas, Physical Review, 1962, 125(3), 795-802.

11. Park, C., "Some Aspects of Chemical Nonequilibrium in High Speed High Temperature Flows," 1964, Ph.D. Thesis, London Univ., London, England.

12. Spitzer, L., Jr., Physical of Fully Ionized Gases, Chap. 5, New York, Interscience Pub., 1956.

13. Cohen, C. B., and E. Reshotko, "The Compressible Laminar Boundary Layer With Heat Transfer and Arbitrary Pressure Gradient," NACA TN 3326, 1955.

14. Stollery, J. L., J. E. Smith, and C. Park, The Effects of Vibrational Relaxation on Hypersonic Nozzle Flows, in the High Temperature Aspects of Hypersonic Flow, AGARDograph 68, W. C. Nelson Ed., New York, Pergamon, 1964, 49-66.

15. Stollery, J. L., and C. Park, Computer Solutions to the Problem of Vibrational Relaxation in Hypersonic Nozzle Flows, Jour. of Fluid Mechanics, 1964, 19(1), 113-123.

16. Bray, K. N. C., "Atomic Recombination in a Hypersonic Wind Tunnel Nozzle," British ARC 20, 562, Nov. 1958.

17. Lighthill, M. J., Dynamics of Dissociating Gas, Jour. of Fluid Mechanics, 1957, 2(1), 1-32.

18. Potter, D. M., Ceramic Coatings, Aircraft Production, 1961, Oct., 354-358 and Nov., 417-421.

19. Goulard, R. J., On Catalytic Recombination Rates in Hypersonic Stagnation Heat Transfer, Jet Propulsion, 1958, 28(11), 737-745.

20. Fay, J. A., and F. R. Riddell, Theory of Stagnation Point Heat Transfer in Dissociated Air, Jour. of Aerospace Sci., 1958, 25(2), 73-85.

21. Yos, J. M., "Transport Properties of Nitrogen, Hydrogen, Oxygen, and Air to 30,000°K," Avco Rep. RAD TM 63-7, 1963.

22. Van Dyke, M., "A Review and Extension of Second-Order Hypersonic Boundary Layer Theory," Stanford Univ. Depart. Aeronautical Rep. 127, 1962.

23. Park, C., Dissociative Relaxation in Viscous Hypersonic Shock Layers, AIAA Jour., 1964, 2(7), 1202-1207.

24. Kemp, N. H., P. H. Rose, and R. W. Detra, Laminar Heat Transfer Around Blunt Bodies in Dissociated Air, Jour. of Aerospace Sci., 1959, 26(7), 421-430.

25. Bond, J. W., Jr., Structure of a Shock Front in Argon, Physical Review, 1957, 105(6), 1683-1694.

26. Adcock, B. D., and W. E. G. Plumtree, On Excitation Temperature Measurements in a Plasma-Jet, and Transition Probabilities for Argon Lines, Jour. Quantitative Spectroscopy and Radiation Transfer, 1964, 4, 29-39.

27. Robben, F., and W. F. Kunkel, Spectroscopic Study of Electron Recombination With Monatomic Ions in a Helium Plasma, Physical Review, 1963, 132(6), 2363-2371.

TABLE I.- SUMMARY OF RESULTS

Type of measurement	Evaluation of individual method of measurement		Comparison of results	
	measured quantity	accuracy	theory backing comparison	result (figure showing comparison)
power-balance method	gross enthalpy	(1) argon: poor** (2) nitrogen: good	none	used as reference
pressure--mass-flow method	gross enthalpy less any unknown latent energy	good	nozzle-flow calculation	(1) argon: agrees with power-balance method (fig. 3) (2) nitrogen: unknown latent energy present (fig. 4)
heat-transfer probe	(1) nozzle exit enthalpy (2) atom or electron concentration at nozzle exit	good	heat-transfer equations including surface catalytic effect	(1) argon: agrees with the above two methods (fig. 5) (2) nitrogen: agrees with power balance (fig. 6)
shock-wave standoff distance	(1) argon: ionic relaxation rate (2) nitrogen: atom concentration at exit	fair	nozzle-flow calculation	(1) argon: agrees with the above (fig. 8) (2) nitrogen: agrees with power balance*** (fig. 9)
radiation	$(\text{electron density})^2$	inaccuracy in referred theory	(1) argon: nozzle-flow calculation and radiation theory of Bond (2) nitrogen: radiation theory of Yos	(1) argon: agrees with the above (fig. 11(a)) (2) nitrogen: indicates metastable species present (fig. 11(b))
spectroscopy*	electron temperature	good	nozzle-flow calculation	(1) argon: agrees with the above (fig. 12) (2) nitrogen: no result

*Carried out by Adcock and Plumtree.[26]
**Due to instrumental error in the tunnel used.
***Resolution poor at low enthalpy levels (see text).

FIGURE TITLES

Fig. 1.- Arrangement of electrodes, settling chamber and nozzle of Imperial College 1-inch plasma-jet wind tunnel.

Fig. 2(a).- Computed variation of ionization fraction and electron temperature along the wind tunnel nozzle for argon, $A_\infty/A^* = 3.5$, $p_o = 0.25$ atm.

Fig. 2(b).- Computed variation of temperature and pressure along the wind tunnel nozzle for argon, $p_o = 0.25$ atm.

Fig. 2(c).- Computed variation of exit conditions with enthalpy level for argon, $A_\infty/A^* = 2.7$, $p_o = 0.25$ atm, for the recombination rates $k = 10k$, k, and $0.1k$.

Fig. 3.- Tunnel head efficiency for argon.

Fig. 4.- Power balance and frozen mass-flow methods compared for nitrogen.

Fig. 5(a).- Results of convective heat-transfer-rate measurement in argon to a cone model.

Fig. 5(b).- Results of convective heat-transfer-rate measurement in argon to a hemisphere model.

Fig. 6(a).- Heat transfer to hemisphere from dissociated nitrogen.

Fig. 6(b).- Heat transfer to 30^o included-angle cone from dissociated nitrogen.

Fig. 7(a).- Typical picture of detached shock wave in argon, $H_t = 1850$ Btu/lb, $\varphi_o = 0$, $\rho_\infty = 0.0014$ amagat.

Fig. 7(b).- Typical microphotodensitometer trace across stagnation region shock layer and the method of determining shock-wave standoff distance, argon.

Fig. 8.- Shock-wave standoff distance of hemisphere in ionized argon, measurement at $\dot{m}$ = 0.15 lb/min.

Fig. 9.- Shock-wave standoff distance of hemisphere in dissociated nitrogen, measurement at $\dot{m}$ = 0.08 lb/min.

Fig. 10.- Arrangement of bolometer in testing position.

Fig. 11(a).- Radiative heat transfer from argon.

Fig. 11(b).- Radiative heat transfer from nitrogen.

Fig. 12.- Comparison of wind-tunnel exit temperature in argon obtained by various methods.

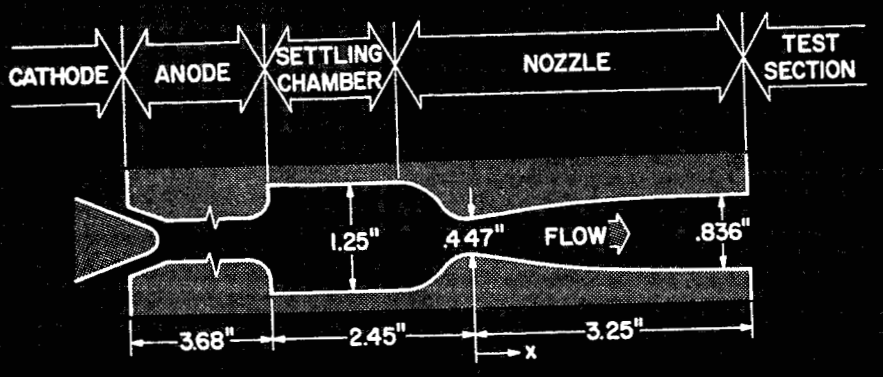
CATHODE
ANODE
SETTLING CHAMBER
NOZZLE
TEST SECTION
1.25"
.447"
FLOW
.836"
3.68"
2.45"
3.25"
x

Fig. 1.

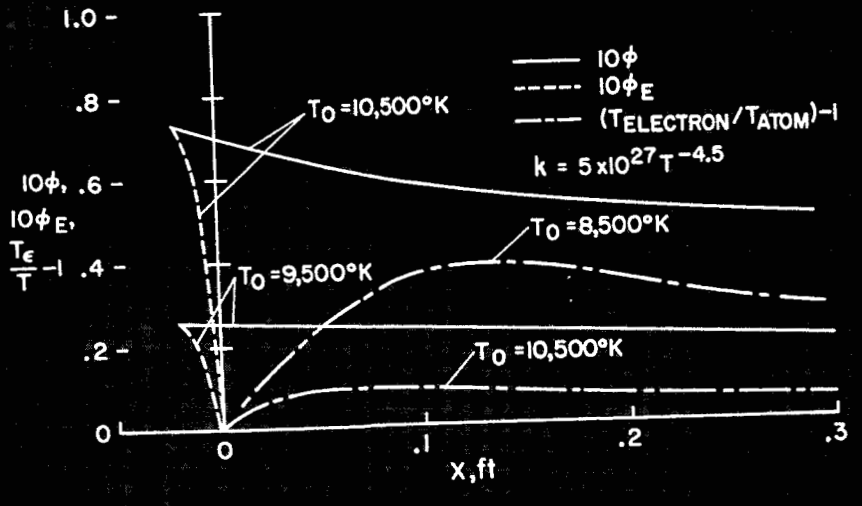
1.0
.8
.6
.4
.2
0
10ϕ, $10\phi_E$, $\frac{T_\epsilon}{T}-1$
10ϕ
$10\phi_E$
$(T_{ELECTRON}/T_{ATOM})-1$
$k = 5 \times 10^{27} T^{-4.5}$
T_0 =10,500°K
T_0 =8,500°K
T_0 =9,500°K
T_0 =10,500°K
0
.1
.2
.3
X, ft

Fig. 2(a).

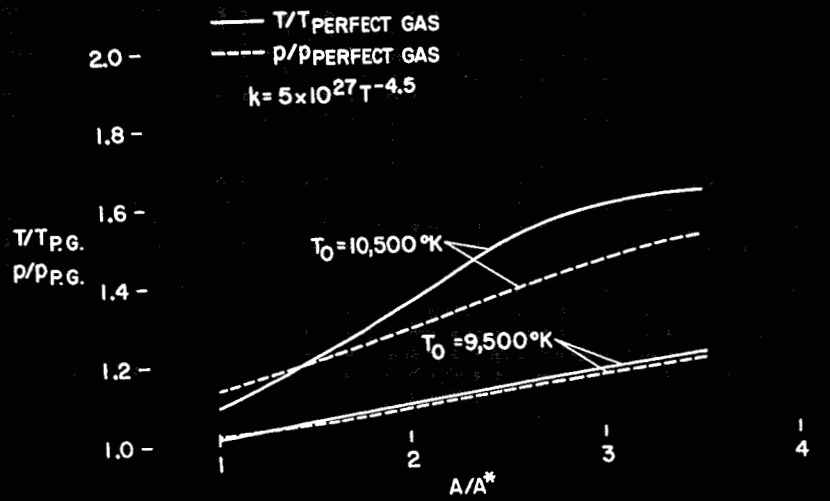
T/T PERFECT GAS
p/p PERFECT GAS
k= 5x10^27 T^-4.5
2.0
1.8
1.6
1.4
1.2
1.0
T/T P.G.
p/p P.G.
T0 = 10,500 °K
T0 = 9,500 °K
1
2
3
4
A/A*

Fig. 2(b).

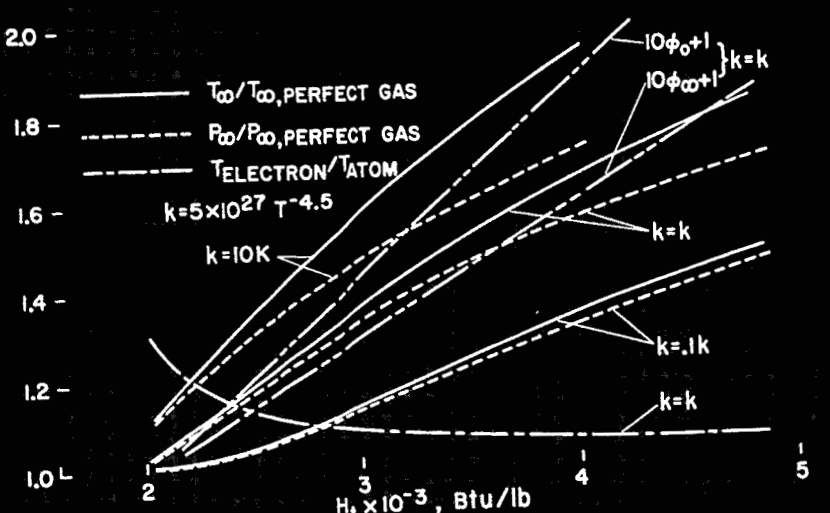
2.0
1.8
1.6
1.4
1.2
1.0
T∞/T∞, PERFECT GAS
P∞/P∞, PERFECT GAS
T ELECTRON/T ATOM
k=5x10^27 T^-4.5
k=10K
10φ0+1
10φ∞+1
k=k
k=k
k=.1k
k=k
2
3
4
5
H1 x10^-3, Btu/lb

Fig. 2(c).

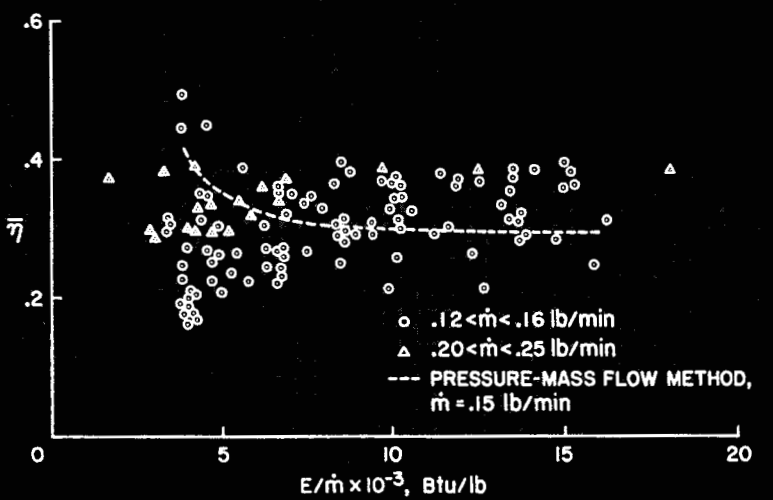
.6
.4
.2
$\bar{\eta}$
0
5
10
15
20
$E/\dot{m} \times 10^{-3}$, Btu/lb
.12<ṁ<.16 lb/min
.20<ṁ<.25 lb/min
PRESSURE-MASS FLOW METHOD, ṁ = .15 lb/min

Fig. 3.

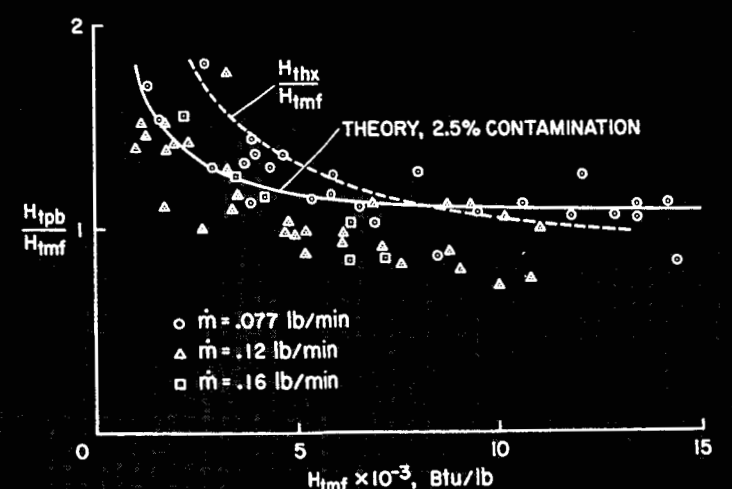
2
1
0
5
10
15
$\frac{H_{tpb}}{H_{tmf}}$
$\frac{H_{thx}}{H_{tmf}}$
THEORY, 2.5% CONTAMINATION
ṁ = .077 lb/min
ṁ = .12 lb/min
ṁ = .16 lb/min
$H_{tmf} \times 10^{-3}$, Btu/lb

Fig. 4.

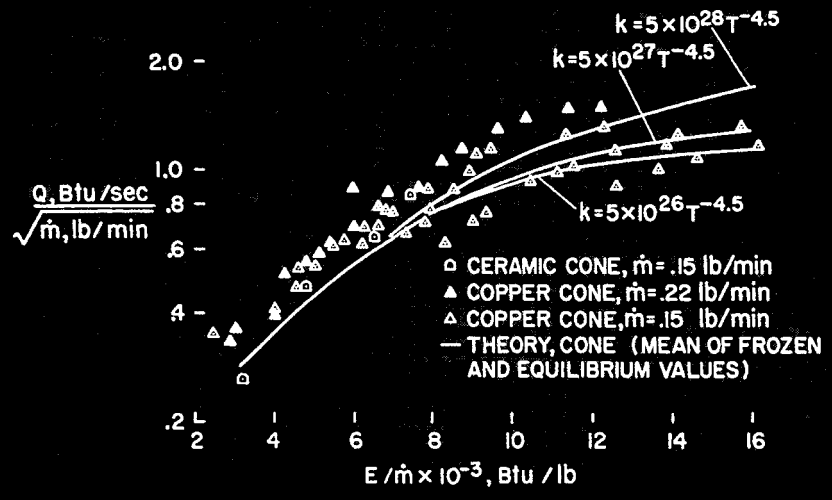
k = 5 × 10^28 T^-4.5
k = 5 × 10^27 T^-4.5
k = 5 × 10^26 T^-4.5
2.0
1.0
.8
.6
.4
.2
Q, Btu/sec / √ṁ, lb/min
CERAMIC CONE, ṁ = .15 lb/min
COPPER CONE, ṁ = .22 lb/min
COPPER CONE, ṁ = .15 lb/min
THEORY, CONE (MEAN OF FROZEN AND EQUILIBRIUM VALUES)
2
4
6
8
10
12
14
16
E/ṁ × 10^-3, Btu/lb

Fig. 5(a).

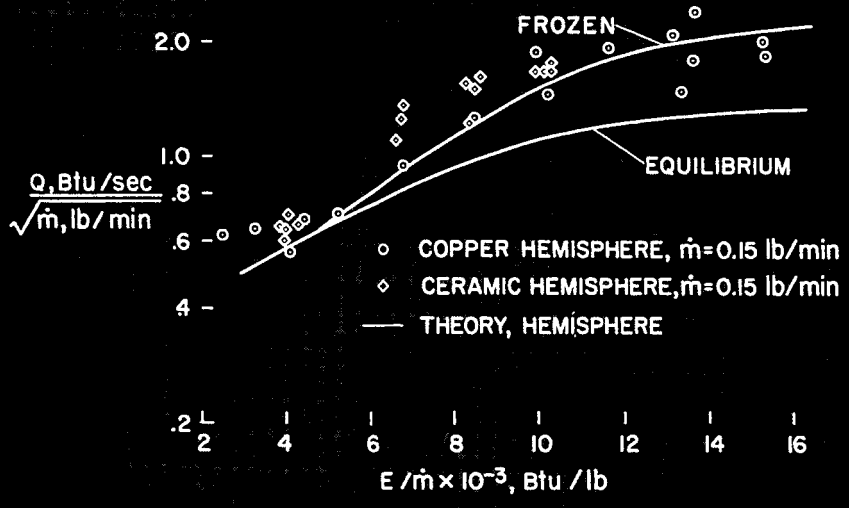
FROZEN
EQUILIBRIUM
2.0
1.0
.8
.6
.4
.2
Q, Btu/sec / √ṁ, lb/min
COPPER HEMISPHERE, ṁ = 0.15 lb/min
CERAMIC HEMISPHERE, ṁ = 0.15 lb/min
THEORY, HEMISPHERE
2
4
6
8
10
12
14
16
E/ṁ × 10^-3, Btu/lb

Fig. 5(b).

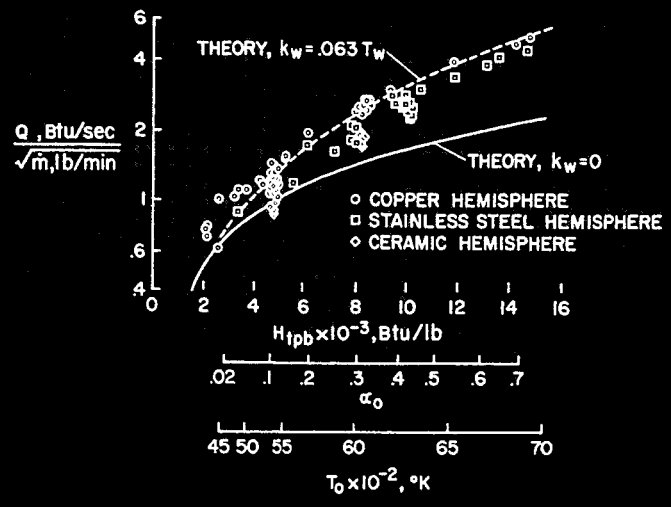
THEORY, $k_w = .063\,T_w$
THEORY, $k_w = 0$
$\frac{Q, \text{Btu/sec}}{\sqrt{\dot{m}, \text{lb/min}}}$
COPPER HEMISPHERE
STAINLESS STEEL HEMISPHERE
CERAMIC HEMISPHERE
$H_{tpb} \times 10^{-3}$, Btu/lb
α_o
$T_o \times 10^{-2}$, °K

Fig. 6(a)

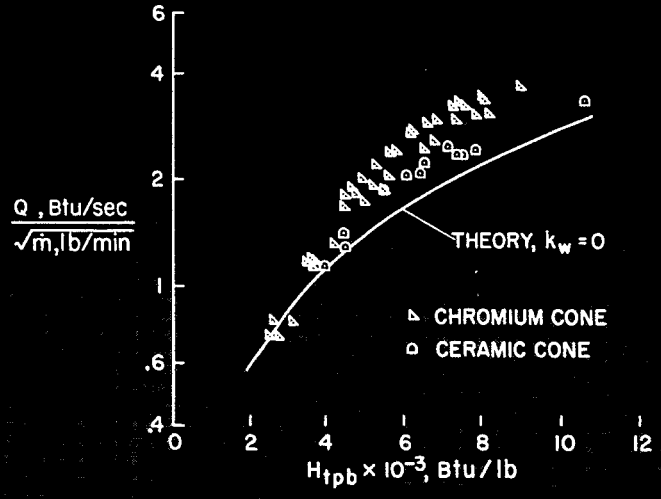
$\frac{Q, \text{Btu/sec}}{\sqrt{\dot{m}, \text{lb/min}}}$
THEORY, $k_w = 0$
CHROMIUM CONE
CERAMIC CONE
$H_{tpb} \times 10^{-3}$, Btu/lb

Fig. 6(b)

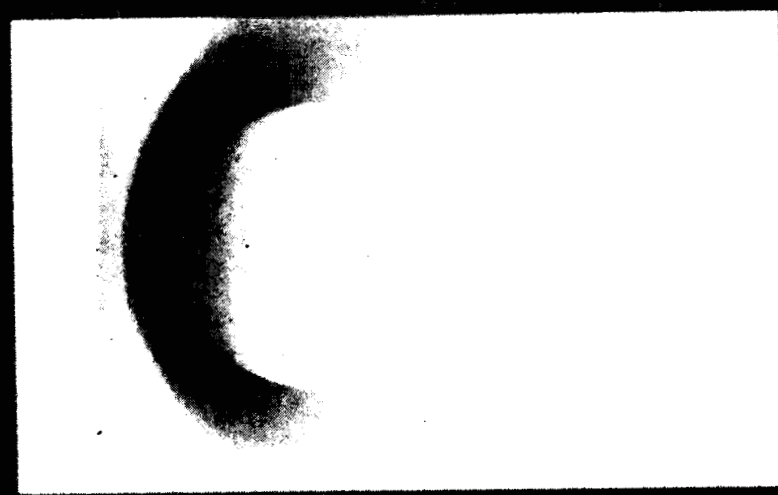

Fig. 7(a)

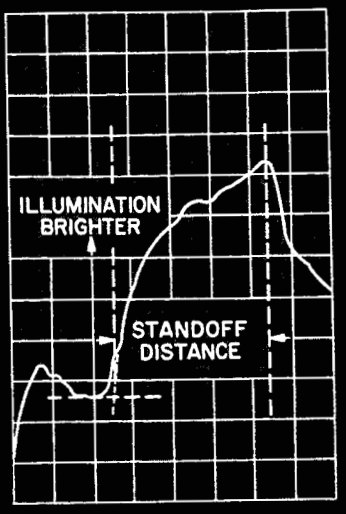
ILLUMINATION BRIGHTER
STANDOFF DISTANCE

Fig. 7(b)

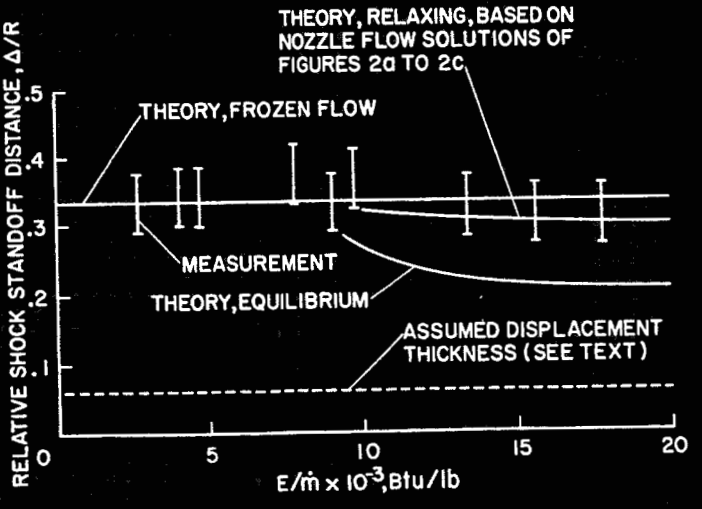
THEORY, RELAXING, BASED ON NOZZLE FLOW SOLUTIONS OF FIGURES 2a TO 2c
THEORY, FROZEN FLOW
MEASUREMENT
THEORY, EQUILIBRIUM
ASSUMED DISPLACEMENT THICKNESS (SEE TEXT)
RELATIVE SHOCK STANDOFF DISTANCE, Δ/R
0
.1
.2
.3
.4
.5
5
10
15
20
E/ṁ x 10⁻³, Btu/lb

Fig. 8

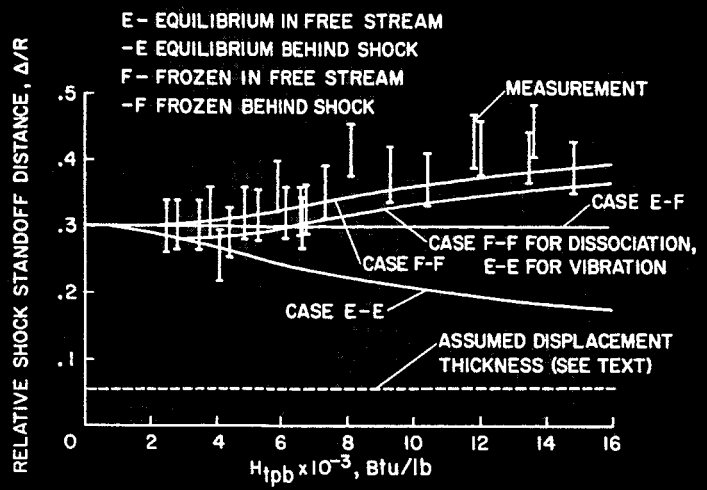
E- EQUILIBRIUM IN FREE STREAM
-E EQUILIBRIUM BEHIND SHOCK
F- FROZEN IN FREE STREAM
-F FROZEN BEHIND SHOCK
MEASUREMENT
CASE E-F
CASE F-F FOR DISSOCIATION, E-E FOR VIBRATION
CASE F-F
CASE E-E
ASSUMED DISPLACEMENT THICKNESS (SEE TEXT)
RELATIVE SHOCK STANDOFF DISTANCE, Δ/R
.5
.4
.3
.2
.1
0
2
4
6
8
10
12
14
16
$H_{tpb} \times 10^{-3}$, Btu/lb

Fig. 9

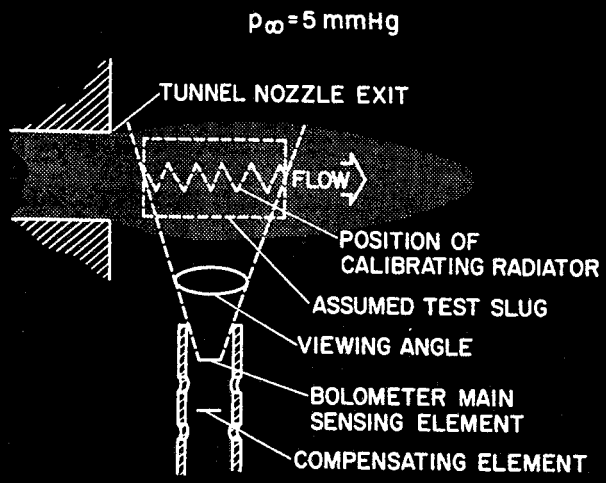
p_∞ = 5 mmHg
TUNNEL NOZZLE EXIT
FLOW
POSITION OF CALIBRATING RADIATOR
ASSUMED TEST SLUG
VIEWING ANGLE
BOLOMETER MAIN SENSING ELEMENT
COMPENSATING ELEMENT

Fig. 10

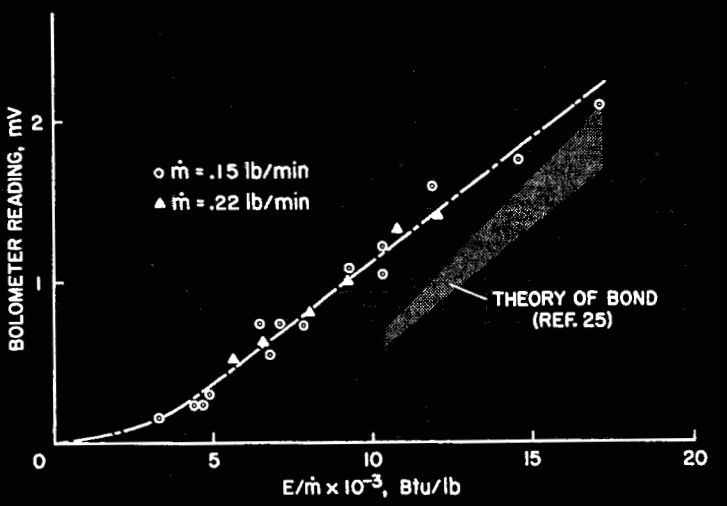

Fig. 11(a)

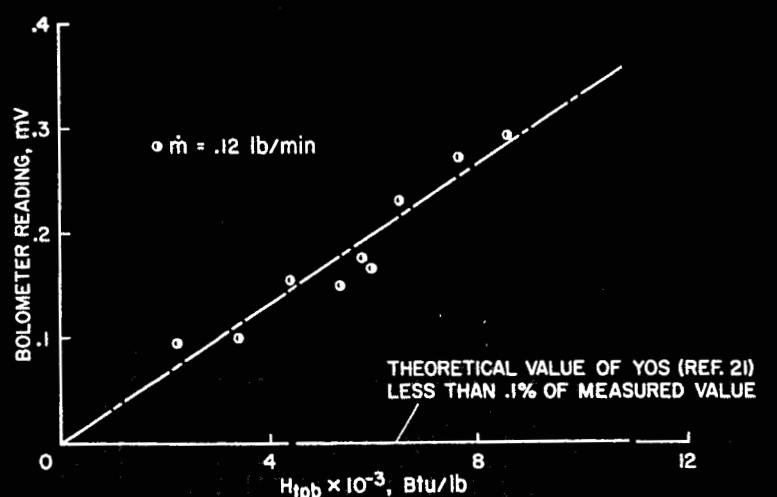

Fig. 11(b)

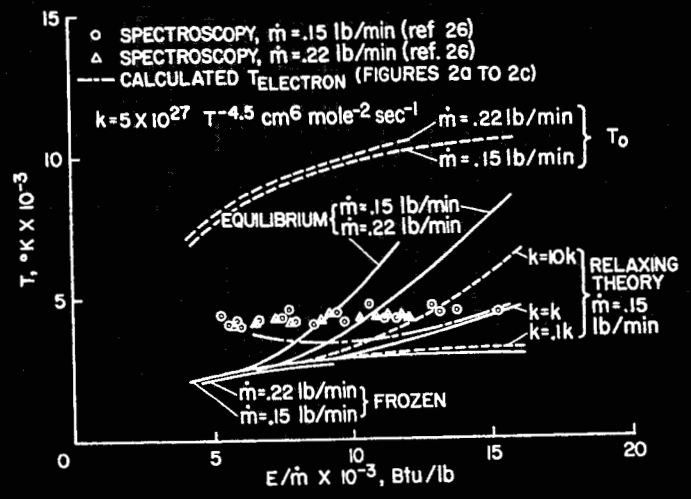
SPECTROSCOPY, ṁ = .15 lb/min (ref 26)
SPECTROSCOPY, ṁ = .22 lb/min (ref. 26)
CALCULATED T ELECTRON (FIGURES 2a TO 2c)
k=5 X 10^27 T^-4.5 cm^6 mole^-2 sec^-1
ṁ = .22 lb/min
ṁ = .15 lb/min
T0
EQUILIBRIUM
ṁ=.15 lb/min
ṁ=.22 lb/min
k=10k
RELAXING THEORY
ṁ=.15 lb/min
k=k
k=.1k
ṁ=.22 lb/min
ṁ=.15 lb/min
FROZEN
T, °K X 10^-3
E/ṁ X 10^-3, Btu/lb
0
5
10
15
20

Fig. 12